



Cooperativity Between Zirconium Dioxide Nanoparticles and Extreme Pressure Additives in Forming Protective Tribofilms: Toward Enabling Low Viscosity Lubricants

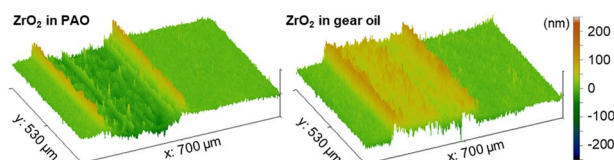
Meagan B. Elinski¹ · Parker LaMascus¹ · Lei Zheng² · Andrew Jackson¹ · Robert J. Wiacek² · Robert W. Carpick¹

Received: 9 July 2020 / Accepted: 24 September 2020 / Published online: 15 October 2020
© Springer Science+Business Media, LLC, part of Springer Nature 2020

Abstract

Realizing the efficiency benefits of low viscosity lubricants requires novel strategies to avoid failures resulting from increased boundary contact. Zirconium dioxide (ZrO_2) nanoparticles (NPs) form protective tribofilms through tribosintering at lubricated contacts in pure hydrocarbon base oils, suggesting they hold promise for reducing boundary contact-induced failures. However, their tribological behavior alongside co-additives found in fully formulated oils has not been examined in depth. Here, the macroscopic tribological performance of dispersed ZrO_2 NPs (1 wt% loading; 5 nm diameter nearly spherical ZrO_2 tetragonal phase NPs with organic capping ligands for oil solubility) with and without the presence of co-additives found in fully formulated commercial gear oils was studied using a mini-traction machine (MTM). The results show that ZrO_2 NPs reproducibly develop surface-bound ~ 100 nm thick tribofilms on both contacting surfaces under a wide range of rolling-sliding contact conditions, from 0 to 100% slide-to-roll ratio. Steady-state traction coefficient values of ZrO_2 tribofilms formed alongside co-additives (0.10–0.11) do not substantially differ from ZrO_2 tribofilms formed in neat polyalphaolefin base oils (0.10–0.13). However, there is improvement in the tribological performance of the contact, with at least a twofold reduction of wear of the steel. This behavior is proposed to be a result of cooperating mechanisms, where the extreme pressure additives adsorbed on the steel surfaces protect them against early adhesive wear, during the time that a protective ZrO_2 tribofilm incorporating the co-additives forms on the steel surfaces, preventing further wear.

Graphic Abstract



Keywords Nanoparticles · Tribofilm · Extreme pressure additives · Tribosintering · Low viscosity gear oil · Co-additives

Electronic supplementary material The online version of this article (<https://doi.org/10.1007/s11249-020-01346-1>) contains supplementary material, which is available to authorized users.

✉ Robert W. Carpick
carpick@seas.upenn.edu

¹ Department of Mechanical Engineering & Applied Mechanics, University of Pennsylvania, Philadelphia, PA 19104, USA

² Pixelligent Technologies LLC, Baltimore, MD 21224, USA

1 Introduction

In the pursuit of higher vehicle efficiency, lower viscosity lubricants are an important and widely targeted means of reducing viscous losses. For hypoid gears in automotive rear axles alone, power losses heavily depend on lubricant viscosity [1], to the extent that lower viscosity gear oils could provide up to 2.5% fuel savings [2]. Approximately 1.5×10^{12} U.S. gallons of petroleum liquid fuels were used worldwide in 2018, with an energy content of 210 EJ (199

quads) [3], so with about 53% being used for transportation [4], a 2.5% fuel savings would translate to a reduction of about 2.8 EJ per year globally.

However, these energy-saving, low viscosity lubricants first require the advancement of antiwear (AW) and extreme pressure (EP) additives, compounds added to oils which improve the protection of parts in sliding contact against failure modes including wear, scuffing, pitting, and micropitting. Lowering the viscosity of lubricants shifts the lubrication regime from elastohydrodynamic lubrication (EHL) towards the mixed and boundary regimes of contact, increasing the frequency and severity of surface contact [5]. Common practice to protect moving components from these lubrication regimes is to enhance the base stock with co-additives [6–8]. Thus, fully formulated oils include (alongside a number of other additives) antiwear (AW) and extreme pressure (EP) additives to combat wear and scuffing. Automotive gear oil AW and EP additives comprise primarily organic compounds including sulfurized olefins such as sulfurized isobutylene or dialkyl pentasulfide and phosphorus-containing compounds such as tricresyl phosphate (TCP) [6–9]. Under the normal operating conditions for high contact stress and high sliding components like hypoid gears, such formulations perform well. However, the increased frequency and severity of mixed and boundary contact conditions that comes with low viscosity lubricants necessitates more durable AW and EP additives, or adopting alternate strategies altogether [2].

Nanoparticle (NP) additives, which are most often inorganic-based, offer a route to more durable protection against failure [10–12]. Extensive possibilities exist for tuning NP chemical composition, physical structure, and lubricating mechanisms [10, 12]. Dai et al. [11] identified seven categories of NP lubricant additives based on composition, and summarized the proposed mechanisms for explaining their tribological performance: laminar sliding of nanosheets; tribofilm formation and adsorption layer formation, which directly alter surface properties and interfacial interactions; shift of the dominant frictional mode from sliding to rolling of NPs; surface repair; and a number of synergistic effects and tribochemical reactions [10, 11]. Any of these beneficial mechanisms, though, do not come without careful consideration of the possible negative impacts of NPs. Effective use of NPs has to surmount challenges such as dispersion stability and abrasiveness [13], and interactions with co-additives required in a fully formulated commercial lubricant can be problematic.

Of the work reviewed by Dai et al. [11], the largest category of NP additives are metal oxides. Zirconium dioxide (ZrO_2) is a particularly attractive additive candidate because its high refractive index enables optically clear dispersions [14, 15], allowing end users to estimate oil quality visually. In tribological measurements,

macroscale tests demonstrate the potential for ZrO_2 NP additives [15–18]. Two recent studies [15, 16] focused specifically on ZrO_2 NPs comprised 5 nm diameter particles with organic ligands bound to the NP surface. Available commercially with high chemical and phase purity and monodispersity, dispersions of these nanoparticles in lubricant base stocks exhibited stability over extended time periods (more than 4 years), in contrast with many other nanoparticles used as oil additives where frequent stirring is required to prevent settling. When suspended in base oil at loadings as low as 0.1 wt%, ZrO_2 additives formed dense, solid, surface-bound tribofilms during mini-traction machine (MTM) tests [15].

In nanoscale tribological tests [16], *in situ* colloidal probe AFM drove and monitored ZrO_2 tribofilm growth in a poly-alphaolefin (PAO) base oil. With the tribofilm growth rate increasing approximately linearly with contact pressure, a triboentering mechanism [19] was proposed for film formation [16]. Moreover, tribofilms developed for all temperatures studied, from -25 to 100 °C, a desirable and wide temperature range for such additives [16]. For example, zinc dialkyldithiophosphate (ZDDP) tribofilms require temperatures of > 50 °C to form durable films [20]. As well, the ZrO_2 NP tribofilms were shown to form on a range of substrates, and consisted almost purely of ZrO_2 [16, 21]. The latter observation shows that tribofilm formation does not require substrate wear, and involves removal of the organic ligands from the surface of the ZrO_2 NPs.

However, these prior studies have only been carried out in pure base oils and thus have not examined the influence that co-additives have on ZrO_2 NP tribofilm formation. Interactions between other NPs and co-additives has been examined in recent studies. For example, Acharya et al. [22] and Khajeh et al. [23] studied the synergistic interactions between organic molecules and NP additives in the formation of a thermal reaction film of tricresyl phosphate with diamonds NPs. Synergistic or cooperative interactions are of course not guaranteed in general, and antagonistic interactions are often seen between commercial additives, setting limits on treat rates of such additives and the conditions and applications for which they can be used [24]. A key example is the known antagonistic interaction in engine oils whereby molybdenum-based friction modifiers like molybdenum dithiocarbamate (MoDTC) inhibit the growth of ZDDP-derived AW films, limiting the amount of MoDTC that can be used to reduce friction [25, 26].

To understand the influence that ZrO_2 -co-additive interactions have on the tribological performance of dispersed ZrO_2 NPs, this study focuses on the behavior of ZrO_2 NP tribofilms in a fully formulated gear oil. A mini-traction machine (MTM) was used to mimic the macroscopic contact of bearings or gears under mixed rolling-sliding conditions. Holding the NP concentration constant (1 wt%), the effect

of both lubricant viscosity and the presence of co-additives were examined for a series of slide-to-roll ratios (SRRs).

2 Experimental Methods

2.1 Lubricant Samples

Pixelligent Technologies LLC provided a series of oil formulations for tribological testing. Synthesis of these ZrO₂ NP additives (PixClear PC14-10-L01) were based on patented solvothermal techniques [27, 28], resulting in highly crystalline ZrO₂ nanocrystals with an average diameter of 5 nm, as determined by transmission electron microscopy (TEM) (Fig. 1a). These NP's are then capped (functionalized) with a proprietary blend of organic ligands to create monodispersed, stable, and optically clear dispersions in a variety of oil formulations. Capping agents, both free and on the nanocrystals, have no additional functionality outside

of the head group that bonds to the nanocrystals (they are non-polar). Dynamic light scattering (DLS) of capped ZrO₂ NPs is measured at 5 wt% concentration in toluene according to the quality control method developed for the commercial product (using organic solvents, in this case toluene for a non-polar nanocrystal). While there would likely be a difference in solvation shell size if DLS measurements were performed for the nanocrystals in, e.g., base oil, the core ZrO₂ NP size would remain the same, separately verified to be 5 nm by TEM. Figure 1b is a typical DLS intensity plot that shows a narrow particle size distribution, with average capped NP size of 9 nm and Dv (99.99) of 18 nm, and showing no aggregation of the ZrO₂ NPs. This average capped NP size of 9 nm represents the hydrodynamic size of the solvated NPs and ligands, in that as-capped and dispersed the 5 nm ZrO₂ nanocrystals are surrounded by a 2 nm ligand/solvation shell. These ZrO₂ NPs are highly crystalline as shown in the X-ray dispersive (XRD) measurement in Fig. 1c. XRD peaks match the Powder Diffraction

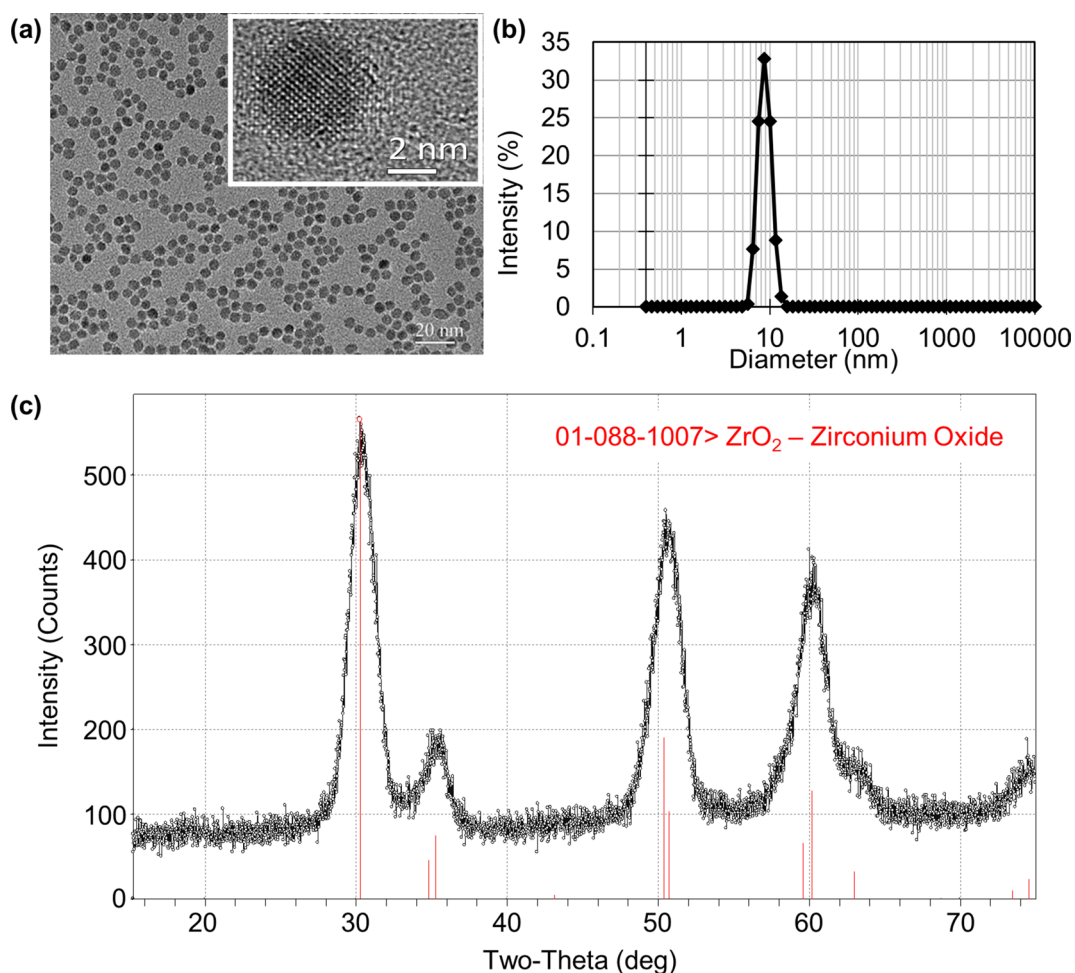


Fig. 1 TEM image **a** of ZrO₂ nanocrystals, with high resolution inset. **b** DLS intensity plot of capped ZrO₂ nanocrystals at 5 wt% in toluene. **c** XRD pattern of ZrO₂ nanocrystals overlaid with the PDF lines of tetragonal ZrO₂

File (PDF) card 01-088-1007, which is for the tetragonal phase of ZrO_2 . Note that fine splitting of each peak, expected for a bulk sample, is not seen due to the well-known peak broadening that occurs in XRD when sampling nanoscale crystallites [29]. Crystallinity of the nanocrystals is also demonstrated in the inset to Fig. 1a, where the crystal planes of a single nanocrystal is shown via high resolution TEM imaging.

Table 1 describes the set of lubricant samples used to compare the behavior of base oils with and without ZrO_2 nanoparticles, and any interactions between ZrO_2 and co-additives. The ZrO_2 samples in PAO were prepared identically as that described in Khare et al. [16] and Thrush et al. [15]. The gear oil samples used were an API Group 3-based automotive gear oil meeting SAE 75W-80 viscosity, with the same additive package as a commercial synthetic SAE 75W-90 gear oil used as a reference in the broader research program of which this study was a part. An additional amount of the proprietary blend of the organic ligands (less than 1% by weight) was added to enhance stability. By eye, there was no observed change in transparency with no observed precipitation of components from the oil. While NP concentration was not specifically optimized for the experiments in this study, 1 wt% loading of the NPs in all oil samples was chosen to balance competing factors. One is that, from a commercial point of view, lower concentrations bring down cost. Therefore, we reduced loading by an order of magnitude from the prior nanoscale work, which used 10 wt% loading [16]. The other factor is that, for fundamental studies, reliable film formation is required. Thrush et al. [15] verified in the MTM this occurred at 0.1 wt% loading in pure base oil, but due to the unknown interactions of the NPs with co-additives, and due to the possibility of lengthening the experimental run time needed to reach steady-state tribofilm thicknesses, we opted for 1 wt%.

For these samples, PAO4, PAO10, and PAO gear oil serve as references without ZrO_2 , the results of which are primarily discussed in Supporting Information Section A. Replicate tests between ZrO_2 +PAO4 and ZrO_2 +PAO10 directly compare the effect of viscosity to better understand tribofilm formation without the presence of co-additives. Meanwhile,

replicate tests comparing ZrO_2 +PAO10 and ZrO_2 +75W-80 provide a direct comparison of the effect of co-additives on tribofilm formation, holding oil viscosity constant. SAE 75W-80 oil, as noted in Table 1, is fully formulated using a conventional gear oil package. The EP additive system is based on phosphorus and sulfur (P/S) containing components resulting in 0.1–0.17 wt% P and 2.0–2.7 wt% S in the finished product.

2.2 Tribological Testing: Mini-Traction Machine and Spacer Layer Imaging

A mini-traction machine (MTM) with spacer layer imaging (SLIM) from PCS Instruments was used for measuring multiple repeats of traction coefficient and tribofilm growth under specified conditions. The test specimens for the MTM tests were new, highly polished 52,100 steel for both the $\frac{3}{4}$ inch (19.05 mm) ball and 46 mm diameter disc specimens. The preparatory cleaning for each ball/disc specimen involved a 15-min sonication through each of acetone, toluene, and 2-propanol. The removable MTM and SLIM components underwent a similar sonication process, spending 15 min successively in acetone, toluene, 0.01 M EDTA (ethylenediaminetetraacetic acid, which helped to wash away residual NPs), and 2-propanol. All parts were wiped with Kimwipe after the cleaning process, with residual fibers removed with compressed nitrogen gas. Separately, the MTM pot and SLIM lid were rinsed in toluene followed by 2-propanol, and dried with compressed nitrogen gas; this rinsing and drying procedure was repeated three times.

All MTM measurements were taken at an applied load of 50 N, yielding a Hertzian maximum contact stress of 1.12 GPa. Traction and Stribeck curves at 40 °C, 60 °C, 80 °C, 100 °C, and 120 °C were taken for all six lubricant samples in Table 1. At 2000 mm/s mean speed, traction curves measured from 0 to 100% SRR exhibited typical temperature-dependent traction coefficient trends for non- ZrO_2 containing samples. Samples with ZrO_2 deviated from expected temperature-dependent behavior when the contact transitioned from EHL to mixed/boundary contact due to increased surface roughness from the tribofilm (from

Table 1 Summary of lubricant samples for mixed rolling-sliding tribological testing

Base oil	Sample label	ZrO_2 content	Co-additive content	Kinematic viscosity (ν) at 100 °C (cSt)
Polyalphaolefin 4	PAO4	–	–	3.9
Polyalphaolefin 4	ZrO_2 +PAO4	1 wt%	–	3.9
Polyalphaolefin 10	PAO10	–	–	10
Polyalphaolefin 10	ZrO_2 +PAO10	1 wt%	–	10
PAO Gear Oil	75W-80	–	P/S package	9.6
PAO Gear Oil	ZrO_2 +75W-80	1 wt%	P/S package	9.6

ca. 5 nm root mean square roughness of the polished steel to 20–40 nm for the films). Stribeck curves at 50% SRR measured from 2000 to 10 mm/s mean speed showed basic temperature and speed dependent behavior, again with the transition from EHL to mixed/boundary contact shifted by the presence of the ZrO₂ tribofilms relative to the non-ZrO₂ containing reference oils. The full set of traction and Stribeck curves are provided and discussed further in Supporting Information Section B.

Based on the traction and Stribeck curves, MTM-SLIM tests were conducted at 100 °C and 150 mm/s entrainment speed to ensure mixed/boundary contact under a range of rolling-sliding conditions. Each 2-h test utilized a new 52,100 steel ball/disc pair. After using triplicate trials to verify that the deviation for values such as traction coefficients and tribofilm thickness was nominally 15%, tests thereafter utilized duplicate trials.

We calculated the elastohydrodynamic film thickness (or minimum film thickness), which, combined with the surface roughness parameters of the contact, yields the specific film thickness, λ (Eq. 1) [5]. The λ values for these MTM conditions (summarized in Table 2) represent the relative ratio of the lubricating film thickness to the surface roughness, indicating the degree of boundary contact. Typically, a lubricated contact with $\lambda < 3$ is considered in the mixed/boundary contact regimes.

$$\lambda = \frac{h_0}{\sqrt{\sigma_B^2 + \sigma_D^2}} \quad (1)$$

In Eq. 1, h_0 is the minimum film thickness, σ_B is the root mean square (RMS) surface roughness of the ball, and σ_D is the RMS surface roughness of the disc. Note that as the tribofilm develops during the MTM test, the surface roughness values will dynamically change, thus the λ values reported in Table 2 are strictly calculated as the values at the start of each test, for the nominal surface roughness of the native, polished, steel-on-steel contact ($\sigma_B = \sigma_D = 5.0 \pm 0.2$ nm). The details showing the calculations are provided in Supporting Information Section C. The uncertainty ranges for the specific film thickness values reported in Table 2 were derived via error propagation based on the standard

Table 2 Summary of the minimum film thickness (h_0) and specific film thickness (λ) for each lubricant sample base oil at 50 N, 150 mm/s entrainment speed, and 100 °C

Base oil	Minimum film thickness (nm)	Specific film thickness
PAO4	6.3	0.897 ± 0.004
PAO10	14.4	2.034 ± 0.008
75W-80	14.0	1.978 ± 0.008

deviation of 5 individual surface roughness measurements of the polished steel contacts (0.2 nm).

Table 3 then summarizes the different ball/disc sliding conditions as a function of slide-to-roll ratio (SRR), dictating the severity of sliding. SRR is defined in Eq. 2 as:

$$SRR = \frac{|u_D - u_B|}{U} \quad (2)$$

where u_B is the ball speed, u_D is the disc speed, and U is the mean rolling speed, or entrainment speed, defined as $(u_B + u_D)/2$.

The rolling/sliding was periodically paused to lift the MTM ball to the SLIM window (loaded onto the lens at 50 N) to capture an interference image. These images were captured at set intervals throughout the test to confirm tribofilm growth, with the focus for analysis here the final image at the end of each 2-h test. The average final film thickness was calculated from an analysis area with a 150 μ m diameter (equal to half the predicted Hertz tribofilm width, ~300 μ m; the diameter of the window of view for the lens is 336 μ m). The thickness values were corrected by a factor of 0.7, a system-specific parameter accounting for both the SLIM lens calibration (for a refractive index of 1.4) and a ZrO₂ refractive index of 2 [30].

2.3 White Light Interferometry

While SLIM measurements provide the tribofilm thickness in situ, SLIM images are obtained using optical interference between the upper and lower surfaces of the translucent tribofilm film and do not provide information regarding any changes in the topography, such as wear or plastic deformation, of the underlying steel ball surface. To gain a quantitative, non-destructive assessment of the degree of wear and the thickness of tribofilms for test specimens, scanning white light interferometry (WLI) of the film surface was used in combination with the SLIM images. The high refractive index of ZrO₂ necessitated reflective coatings on the tribofilms for accurate scanning WLI measurements [31]. A Cressington Sputter Coater 108 was used to coat the test specimens using a Au/Pd target. MTM ball specimens were

Table 3 Summary of MTM testing conditions at 50 N applied load, 150 mm/s entrainment speed, and 100 °C

SRR (%)	Ball speed (mm/s)	Disc speed (mm/s)	Sliding speed (mm/s)
0	150.0	150.0	0.0
25	131.3	168.8	37.5
50	112.5	187.5	75.0
100	75.0	225.0	150.0

coated for 30 s at a 0.15 mbar vacuum pressure, yielding a AuPd-coating thickness estimated to be 20–40 nm.

Scanning WLI images were taken on a Zygo NewView 6300 Interferometer with a 20× objective and 0.5× internal multiplier, yielding a magnification level of 10× and a 530 μm × 700 μm field of view. For the MTM balls, the tribofilm was oriented to the apex of the ball, centered under the objective, and imaged with a vertical scan range of 150 μm. Images were leveled through a spherical subtraction in the software program Gwyddion [32]. From the processed data, an average step-edge height was calculated as the tribofilm height minus the steel height (with the tribofilm and steel heights calculated as the average values over respective 150 μm × 150 μm areas).

2.4 Raman Spectroscopy

Raman spectroscopy was used for chemical characterization of the tribofilms. With a NT-MDT NTEGRA Spectra confocal Raman microscope equipped with an Andor Peltier cooled CCD detector, a 491 nm laser was focused to the sample through a 100× objective.

2.5 Secondary Ion Mass Spectrometry Depth Profiles

Even though WLI yields step-edge height, and Raman spectroscopy yields chemical composition of the bulk tribofilm, neither of these techniques could demonstrate that the co-additives were incorporated through the entire tribofilm depth, so secondary ion mass spectrometry (SIMS) depth profiling was used to determine this. Representative ZrO₂+PAO4 and ZrO₂+75W-80 tribofilms formed at a 50% SRR were sent to Evans Analytical Group (EAG) Laboratories for SIMS depth profiling. Due to sample size constraints, 4 mm × 6 mm sections were cut from the disc specimens.

3 Results and Discussion

3.1 Traction Coefficient Behavior and Tribofilm Thickness as a Function of Slide-to-Roll Ratio

The traction coefficient behavior over time for each ZrO₂ sample and SRR combination is plotted in Fig. 2a–c. The traction coefficient data for the non-ZrO₂ containing reference oils are in Fig. 2d–f, and Table 4 provides a summary of traction coefficient behavior to compare non-ZrO₂ and ZrO₂ containing oils.

Figure 2a–c show that similar trends develop across all ZrO₂-containing oil formulations and slide-to-roll ratios: for SRRs > 0%, a starting traction coefficient of nominally

0.03–0.05 initially increases as the tribofilm develops, before reaching a steady-state value in the 0.10–0.13 range. For the 50% SRR trials in PAO4, the traction coefficient behavior is consistent with a recent report from Thrush et al. [15] For the 0% SRR trials (both ZrO₂-containing in Fig. 2a–c and non-ZrO₂ containing in Fig. 2d–f), non-zero traction coefficient values of 0.01–0.03 were observed, but simply reflect that spurious microslips prevent pure rolling conditions.

In contrast to samples with ZrO₂ NPs that exhibited nominally similar trends in traction coefficient, the tribological behavior for the reference oils varied based on viscosity and formulation. For PAO4 (Fig. 2d) at a 50% SRR, the conditions were severe enough that the ball and disc seized together within the first three minutes, causing a rapid rise in traction coefficient and exceeding the measurement capabilities of the instrument, terminating the trial. For PAO10 (Fig. 2e) at a 50% SRR there is early irregularity in the traction coefficient behavior, but the test continued to run with a steady increase in traction coefficient associated with wear (see later discussions on surface morphology, Fig. 6). As a fully formulated gear oil, 75W-80 maintains steady traction coefficient behavior for all SRRs tested, with only slight run-in (Fig. 2f). Comparing the oils without and with ZrO₂, ZrO₂ NPs are able to prevent substantial damage to the steel interface in pure PAO4 and PAO10, an important tribological attribute that is in agreement with MTM work by Thrush et al. [15] and supports observed macroscale anti-scuffing behavior of ZrO₂ in 75W-80 recently reported by Demas et al. [33].

By closer examination of the ZrO₂-containing samples (Fig. 2a–c), the evolution of traction coefficient is seen to be influenced by both the oil viscosity and the presence of co-additives. Comparing ZrO₂+PAO4 to ZrO₂+PAO10 (both with no co-additives), the ZrO₂+PAO4 formulation has an overall higher (albeit irregular) rate of increase in the traction coefficient for the first 30 min of testing than ZrO₂+PAO10, likely due to the lower viscosity and corresponding lower λ value. Comparing the two samples with similar viscosities (ZrO₂+PAO10 to ZrO₂+75W-80), the presence of co-additives in the 75W-80 gear oil also accelerates the rate of increase in traction coefficient in the early stages of testing. Tribofilm growth rates strongly influence traction coefficient evolution; a more quantitative study of tribofilm growth kinetics will be the subject of future work. Overall, it is clear that surface-adsorbed co-additives do not hinder the growth of ZrO₂ NP-derived AW tribofilms.

The steady-state traction coefficient values obtained allow us to compare ZrO₂-containing oils with other alternatives. The 0.10–0.13 range of ZrO₂-containing oils is two to three times higher than the 0.03–0.05 values of base oil alone, but merely reflects the boundary traction coefficient value of the ZrO₂ tribofilm compared to the mixed lubrication for the base oil. The transition from mixed to primarily boundary

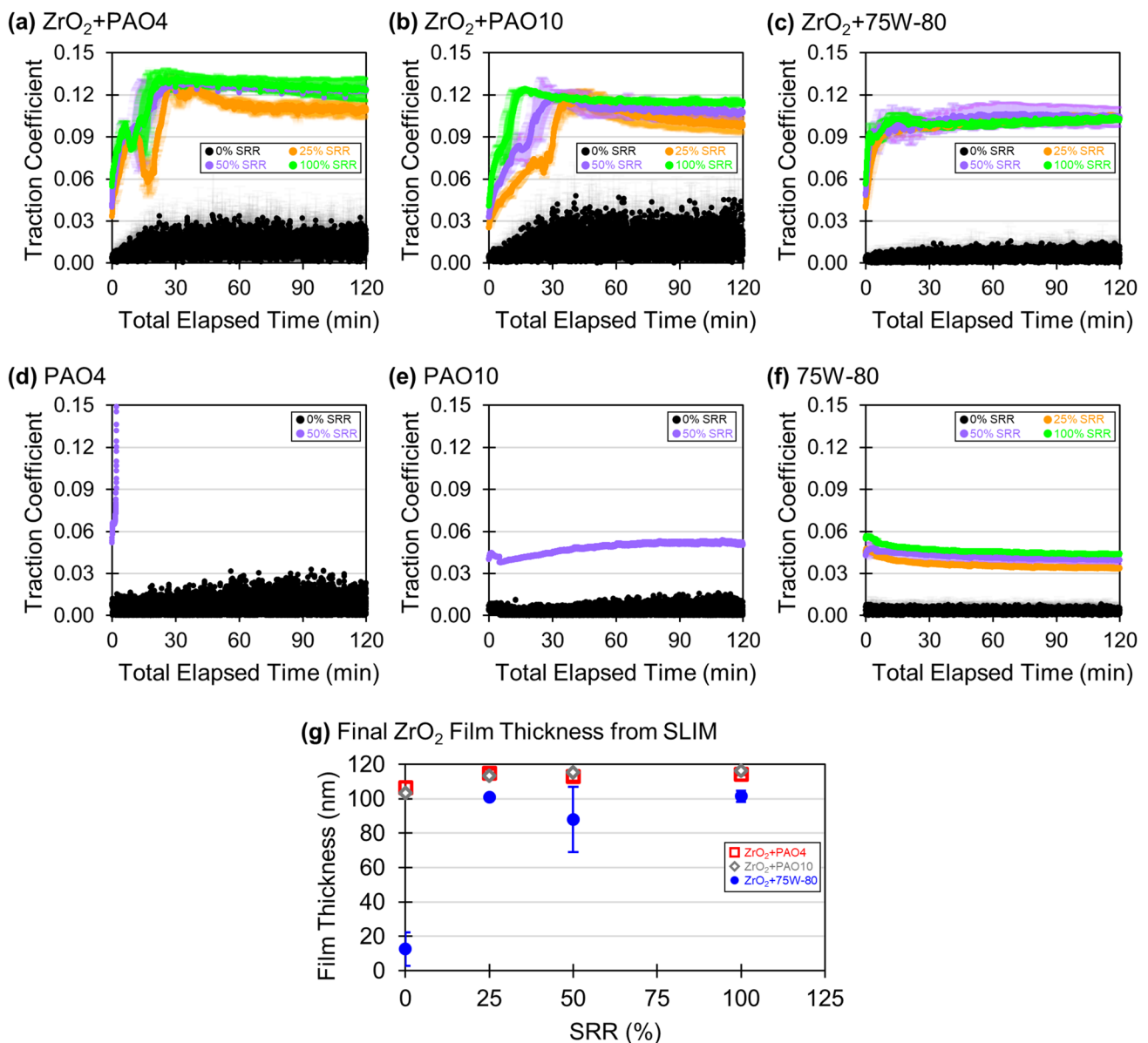


Fig. 2 Traction coefficient values measured in the MTM (at 100 °C, 1.12 GPa, and 150 mm/s entrainment speed) over time at different SRRs for **a** ZrO₂+PAO4, **b** ZrO₂+PAO10, and **c** ZrO₂+75W-80. In **a–c**, the black curves are for 0% SRR, the orange curves are for 25% SRR, the purple curves are for 50% SRR, and the green curves are for 100% SRR. The corresponding shaded areas for each curve represent the standard deviations. The non-ZrO₂ containing oils are in **(d–f)**. Due to excessive sample damage, PAO4 **(d)** and PAO10 **(e)** tests were

reduced to one trial each at 0% SRR (black) and 50% SRR (purple). 75W-80 **f** was tested for two trials at each SRR, with the same color labeling as in **(a–c)**. The final MTM ball tribofilm thicknesses (at the end of each test in **a–c**) measured by SLIM for each sample/SRR is plotted in **(g)**. In **g**, the ZrO₂ samples are ZrO₂+PAO4: red squares, ZrO₂+PAO10: gray diamonds, and ZrO₂+75W-80: blue circles (Color figure online)

contact is attributable to the increase in surface roughness as the tribofilm develops, from ca. 5 nm RMS of the polished steel contacts (λ range 0.897–2.034, Table 2) to 20–40 nm RMS for the ZrO₂ tribofilms. Accounting for varying surface roughness for each oil viscosity, the final λ values for the ZrO₂ samples span a range of 0.112 for ZrO₂+PAO4 at 40 nm RMS up to 0.509 for ZrO₂+PAO10 at 20 nm RMS. Additionally, with severe enough conditions that there is

primarily boundary contact, there is no substantial dependence in the tribofilm traction coefficient based on oil viscosity. This seemingly high traction coefficient range compares well to α -ZrP nanoplatelets [34] for example, and various forms of ZDDP (although a direct comparison between the measurements here and other studies cannot be made due to differences in measurement methods and conditions) [31]. When sufficient speeds are reached to move towards the EHL

Table 4 General summary of traction coefficient behavior of non-ZrO₂ containing oils (Fig. 2d–f) and ZrO₂-containing oils (Fig. 2a–c)

Base oil	SRR (%)	Steady-state traction coeff. without ZrO ₂	Steady-state traction coeff. with ZrO ₂
PAO4	25	(not tested)	0.11–0.13
	50	Seized within 1st 3 min	0.11–0.13
	100	(not tested)	0.11–0.13
PAO10	25	(not tested)	0.10–0.12
	50	0.05	0.10–0.12
	100	(not tested)	0.10–0.12
75W-80	25, 50, 100	0.03–0.05	0.10–0.11

0% SRR values are excluded from the table, but are shown in Fig. 2

regime as seen in the MTM Stribeck curves (Supporting Information Section B), the traction coefficient decreases, even reaching sub-0.06 for ZrO₂+75W-80 at a 2000 mm/s entrainment speed. Higher entrainment speeds were not possible due to motor speed limitations of the MTM instrument, but it is reasonable to expect that the traction coefficient values for the ZrO₂ samples would continue to decrease to the similar EHL traction coefficient values measured for the non-ZrO₂ containing oils.

The decrease in traction coefficient with increasing entrainment speed (higher λ values) indicates that neither the ZrO₂ tribofilm nor the dispersed ZrO₂ NPs significantly impact the base oil's EHL traction coefficient. Consistent with this finding, viscosity measurements from Thrush et al. [15] found that a 1 wt% dispersion of ZrO₂ in PAO4 increased low shear rate kinematic viscosity by only 4.7% at 100 °C. This finding has consequences for considering the use of these NPs to enable low viscosity gear oils, as it suggests that lower viscosity oils can maintain efficiency improvements when operating in the EHL regime without substantial rheological interference of the NP additives, while the tribofilms can provide the needed protection against failure when conditions drive the operating regime towards boundary contact. Regarding system efficiency, even with the higher traction coefficient associated with the ZrO₂ tribofilm relative to the gear oil alone we still anticipate there to be overall efficiency benefits gained from the use of low viscosity oils. The majority of operating conditions, for gearboxes for example, will still be in the EHL regime, where the reduction of churning losses will outweigh efficiency reductions associated with the relatively higher tribofilm traction coefficient. Further, an aspect of future work on this project includes examining compatible friction modifiers for the ZrO₂ tribofilms that will lower boundary contact friction and improve overall efficiency.

At the end of each two-hour test, the final tribofilm thickness was measured in situ via SLIM. Figure 2g shows that nearly all ZrO₂ samples, regardless of oil formulation or

SRR, developed thick AW tribofilms, in agreement with recent MTM-SLIM work for ZrO₂+PAO4 [15]. These films were thinnest for ZrO₂+75W-80, but in general ranged from 100 to 120 nm. The exception to the 100–120 nm tribofilm thickness is for ZrO₂+75W-80 at a 0% SRR, which only forms a 13 ± 10 nm thick tribofilm. This observation may be explained by assuming that, without sliding, the surface-adsorbed co-additives in 75W-80 inhibit tribofilm nucleation or growth, whereas sliding enhances tribofilm nucleation through mechanical action. It is possible that the mechanical action of sliding, for example, promotes removal of the capping ligands [16], promotes transport of NPs to nucleation sites within the contact, or increases the total energy driven into the contact to compress NPs into the substrate or to sinter with each other. An alternate possibility is that if the microslips observed at 0% SRR (evidenced by the non-zero traction coefficient) are related to friction within the contact, the steel-on-steel contact in PAO could have high friction helping tribofilm nucleation, but the friction is lowered in 75W-80 in the presence of the P/S additives, reducing tribofilm nucleation. Further work is required to clarify these issues. Regardless of cause, for SRRs > 0%, minimal difference in film thickness is seen between the 75W-80 and PAO samples. It is also worth noting that, while it is possible SLIM overestimates tribofilm thickness due to tribofilm surface roughness preventing full conformation to the SLIM lens [31], a systematic offset in the absolute values of reported tribofilm thicknesses would not change the observed trends or conclusions for the presented data. The full set of SLIM images, along with additional scanning electron microscopy images and elemental analysis from energy dispersive X-ray spectroscopy on representative tribofilms formed at a 50% SRR, are provided in Supporting Information Section D.

3.2 Tribofilm Morphology

To more closely examine differences in tribofilm formation, ex situ WLI measurements were taken on the AuPd-coated specimens after the MTM tests were completed. Unlike SLIM images, which are based on refraction, WLI generates interference images from reflection, so the WLI measurements on the AuPd-coated specimens reveal tribofilm step-edge height with respect to the surrounding steel surface. They can also be performed on both the balls and discs, while the SLIM images are only taken on the balls. Figure 3 shows representative topographic images of the ball specimens for each sample/SRR combination, corrected for spherical curvature. The corresponding disc data reveal different tribofilm morphologies than the ball samples. Briefly, we attribute this in part to the fact that different ball vs. disc velocities may unequally affect wear and material transfer rates, further complicated by the level of protection

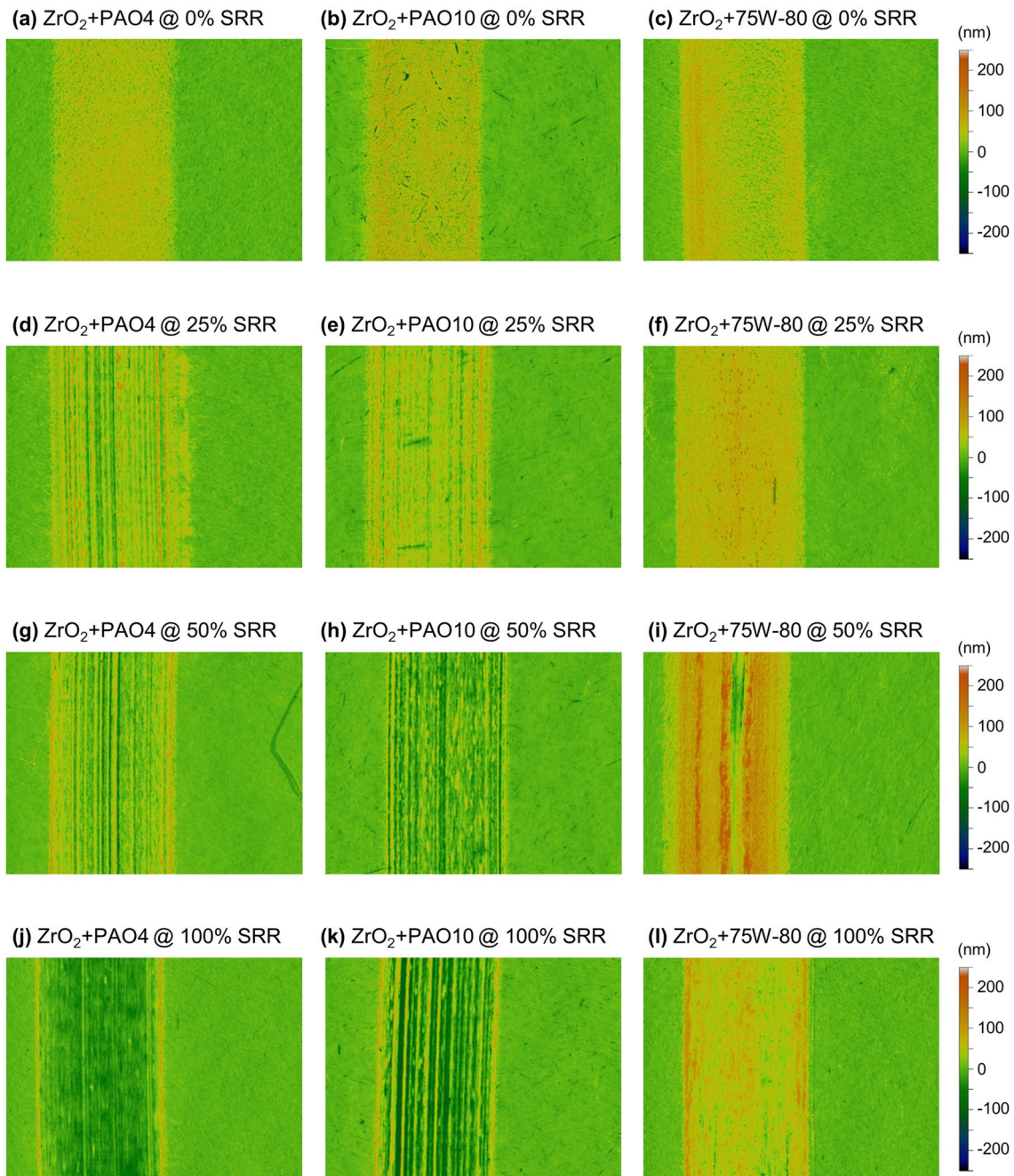


Fig. 3 White light interferometry (WLI) images ($700\ \mu\text{m}\times 530\ \mu\text{m}$, $\pm 250\ \text{nm}$ z-scale), corrected for spherical curvature, for AuPd-coated MTM ball specimens after MTM tests conducted for 2 h at $100\ ^\circ\text{C}$, $1.12\ \text{GPa}$, and $150\ \text{mm/s}$ entrainment speed.

Images **a–c** show the tribofilms formed at 0% SRR for $\text{ZrO}_2+\text{PAO4}$, $\text{ZrO}_2+\text{PAO10}$, and $\text{ZrO}_2+75\text{W-80}$, respectively. Similarly, **d–f** show the 25% SRR trials, **g–i** show the 50% SRR trials, and **j–l** show the 100% SRR trials

afforded to the steel interface (e.g., in PAO or in the presence of 75W-80 additives) at the very onset of the tests before a ZrO_2 -based tribofilm has time to develop. These issues are discussed further in Supporting Information Section E.

First we summarize the tribofilm morphology results qualitatively. The 0% SRR cases (Fig. 3a–c) show that ZrO_2 films formed even under rolling conditions, consistent with

the SLIM data (Fig. 2g). That ZrO_2 NPs do not require substantial shear stress to form tribofilms supports previous reports that a tribosintering mechanism drives ZrO_2 tribofilm formation [16], whereby the normal stress alone is sufficient to compact NPs into sintered films in the contact region. This stands in contrast to other additives, such as the AW additive ZDDP (used primarily in engines) which

requires shear stress to drive development of a solid tribofilm [20, 35].

As the chosen degree of sliding is increased, more differences in tribofilm morphology emerge as a function of the lubricant composition. For ZrO_2 +PAO4, while the SLIM images indicate consistently thick tribofilms (Figs. 2g and S4), the step-edge heights determined from WLI (Fig. 3a,d,g,j) decrease with increased SRR (increasing sliding severity). In the most severe case at 100% SRR (Fig. 3j), the tribofilm has a predominantly net-negative step-edge height. Figure 4 further illustrates the different film morphologies for the ZrO_2 oil formulations relative to the surrounding steel for the most severe sliding conditions tested (100% SRR). The 3D projections (Fig. 4a–c) of the WLI images shown in Fig. 3j–l along with the corresponding cross sections (Fig. 4d) highlight how tribofilms have developed within a wear track on the steel ball, and is most pronounced for the ZrO_2 +PAO4 sample.

To help clarify the appearance of the WLI images, note that in Figs. 3 and 4, because the spherical curvature of the balls has been subtracted, running tracks that appear sunken in shape (e.g., Figure 3j) actually reflect the ball surface being slightly polished to a flat finish. Also note the relative dimensions of the image magnify the appearance of any net-negative (e.g., the concave shape in Fig. 3j)

or net-positive (e.g., the raised track in Fig. 3i) step-edge features, with $700\ \mu\text{m} \times 530\ \mu\text{m}$ x- and -y-dimensions compared to a $\pm 250\ \text{nm}$ height range. For context, Fig. 5 shows a representative WLI image of ZrO_2 +PAO4 at 100% SRR (the same image in Fig. 3j) before correction for the spherical curvature of the ball. In the cross section shown in Fig. 5b, the slight polish to the ball relative to its overall curvature is orders of magnitude smaller. Thus, in order to meaningfully analyze the running track, the background curvature of the ball must be subtracted. Applying a consistent analysis method of masking the running track region before the background subtraction produced the series of images shown in Fig. 3, with distinct step-edge features against a flat background. The tribofilms being offset to varying degrees from the center of the WLI images (and the apparent apex of the ball) is only a consequence of small offsets in alignment under the WLI objective and does not reflect any misalignment in the MTM, nor does it impact the image analysis.

The existence of a tribofilm on an apparently worn ball surface is attributable either to abrasive wear [5, 36, 37] or to material loss by adhesive wear in the harsh steel-on-steel sliding, either or both of which occur first, after which the ZrO_2 tribofilm grows. This is supported by the MTM traction coefficient and surface morphology data for the pure oils, and is especially evident in the traction coefficient

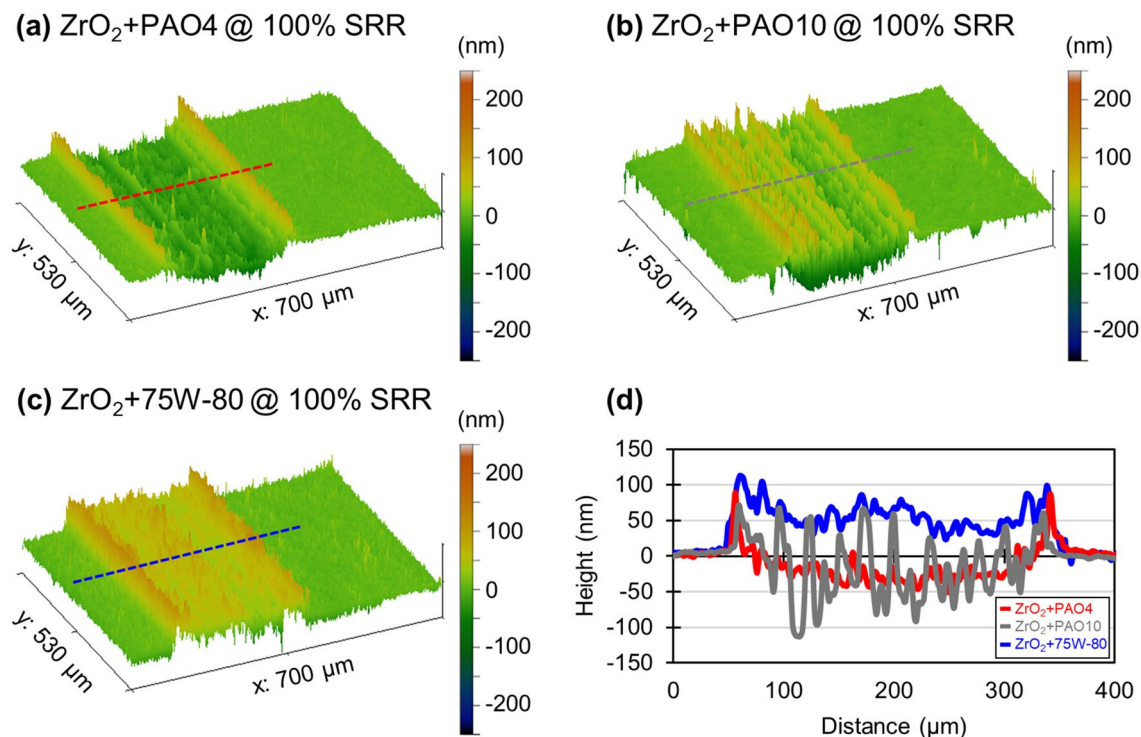


Fig. 4 3D projects of the WLI images (corrected for spherical curvature) shown in Fig. 3j,k,l for tribofilms formed at 100% SRR: **a** ZrO_2 +PAO4, **b** ZrO_2 +PAO10, and **c** ZrO_2 +75W-80. The dashed

lines in **a–c** indicate the cross sections taken for a 50-line average, overlaid in **d** with red for ZrO_2 +PAO4, gray for ZrO_2 +PAO10, and blue for ZrO_2 +75W-80 (Color figure online)

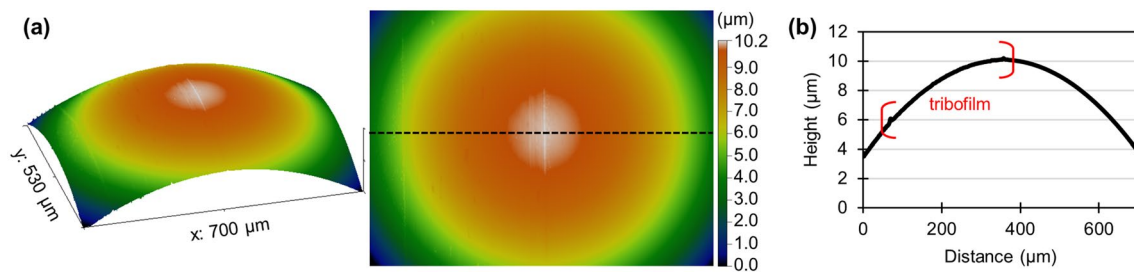


Fig. 5 **a** WLI image (3D and 2D view) of AuPd-coated MTM ball before spherical background subtraction (sample specimen: ZrO_2 +PAO4 tested at 100% SRR, for 2 h, 100 °C, 1.12 GPa, and 150 mm/s entrainment speed). The dashed line in the 2D image

shows where the 50-line averaged cross section plotted in **b** was taken. The red brackets in **b** denote the edges of tribofilm (Color figure online)

data in Fig. 2d,e, which indicate that wear occurs for pure PAO4 and PAO10. At 0% SRR, pure PAO4 and PAO10 have non-zero traction coefficients increasing slightly over time, indicative of increasing wear. At 50% SRR, pure PAO4 seized within the first three minutes of testing, causing a spike in traction coefficient and the test to terminate. At 50% SRR, the traction coefficient for pure PAO10 increased over time, again indicative of increasing wear (note, however, the traction coefficient increase for PAO10 at 50% SRR was to 0.05–0.06, not the 0.12 value associated with the ZrO_2 tribofilm).

The observation of wear underlying a tribofilm discussed in Fig. 4 is also supported by the WLI data in Figs. 6 and 7 which illustrate the changes in the steel surface that occur when no nanoparticles are present. For PAO4 at 0% SRR, Fig. 6a,b shows adhesive wear with material transfer from the disc to the ball. When PAO4 was tested at a 50% SRR (Fig. 6c,d), as mentioned above, the ball and disc specimens quickly seized (Fig. 2d) with substantial material transfer from the ball to the disc observed. For PAO10 at 0% SRR, similar wear behavior as for the PAO4 at 0% SRR is seen across the interface (Fig. 6e,f), with material transferred from the ball to the disc albeit less than for PAO4, as expected for a higher viscosity lubricant. At a 50% SRR, both ball and disc surfaces tested in PAO10 (Fig. 6g,h) show a mix of wear modes (scuffing, pitting, material transfer). Note that for PAO4 and PAO10, testing was reduced to one trial each at 0% SRR and 50% SRR due to the destructive sliding behavior.

For the fully formulated 75W-80 gear oil, two trials were run at each SRR (0%, 25%, 50%, and 100% SRR). Figure 7 focuses on 0% and 50% SRR for comparison with the PAO oils (the 75W-80 25% SRR and 100% SRR results are in Supporting Information Section A). Negligible surface change was observed for low SRRs (0%) on the ball surface (Fig. 7a), with some pitting and wear scars observed on the disc surface (Fig. 7b). In more severe sliding cases (50% SRR), occasional wear scars were observed

on both ball and disc surfaces (Fig. 7c,d), 20–50 nm deep and 10–20 μ m wide. It was notable that there was much less damage than was seen with the pure PAO tests.

The ZrO_2 -free results discussed for Figs. 6 and 7 help explain differences in the behaviors of ZrO_2 +PAO4, ZrO_2 +PAO10, and ZrO_2 +75W-80, which are seen in Fig. 3. For ZrO_2 +PAO4 (Fig. 3a,d,g,j) compared with ZrO_2 +PAO10 (Fig. 3b,e,h,k), which is a higher viscosity lubricant than ZrO_2 +PAO4 but still has no other co-additives, we observe that there is a similar effect of an increase in underlying surface wear with increasing SRR. However, some differences are apparent in the tribofilm morphology. For example, at 100% SRR, the ZrO_2 +PAO10 film (Figs. 3k, 4b) has an increased prevalence of raised and lowered grooves compared to ZrO_2 +PAO4. This morphology difference is likely due to the difference in starting λ values. For the higher λ value (PAO10), fewer surface asperities are initially in contact than for the lower λ value (PAO4), leading to the nucleation and development of a more striated, i.e., less uniform morphology.

For the ZrO_2 in two PAO samples (Figs. 3a,d,g,j and b,e,h,k), especially for the higher viscosity ZrO_2 +PAO10, compared with ZrO_2 +75W-80 gear oil (Fig. 3c,f,i,l), the observed differences suggest a distinct and beneficial effect between the ZrO_2 NPs and the P/S additive package of the gear oil. Qualitatively, for ZrO_2 +75W-80 at 25%, 50%, and 100% SRRs (Fig. 3f,i,l), there is a net-positive step-edge height for the tribofilm formed under each of these conditions. This is the most apparent for the tribofilms formed at 100% SRR, with ZrO_2 +75W-80 (Figs. 3l, 4c) forming a clear raised film compared to ZrO_2 +PAO4 and ZrO_2 +PAO10 (see Fig. 4d for a comparison of the three). With film thickness values measured via SLIM similar to the PAO+ ZrO_2 samples, this implies there is significantly less underlying wear of the substrate. This indicates that the AW enhancement due to the presence of co-additives is preserved in the presence of ZrO_2 , and the ZrO_2 -based tribofilm is then still able to form on the substrate.

Fig. 6 WLI images ($700\ \mu\text{m} \times 530\ \mu\text{m}$, $\pm 250\ \text{nm}$ z-scale) for AuPd-coated MTM ball specimens (corrected for spherical curvature) and AuPd-coated disc specimens ran in PAO oils at $100\ ^\circ\text{C}$, $1.12\ \text{GPa}$, and $150\ \text{mm/s}$ entrainment speed. Images **a**, **b** show wear of the ball and disc steel surfaces, respectively, ran at 0% SRR in PAO4. Images **c**, **d** similarly show the ball/disc pair ran at 50% SRR in PAO4. Images **e–h** show the samples that were ran in PAO10, with the ball/disc surfaces tested at 0% SRR in **e**, **f** and the ball/disc surfaces tested at 50% SRR in **g**, **h**

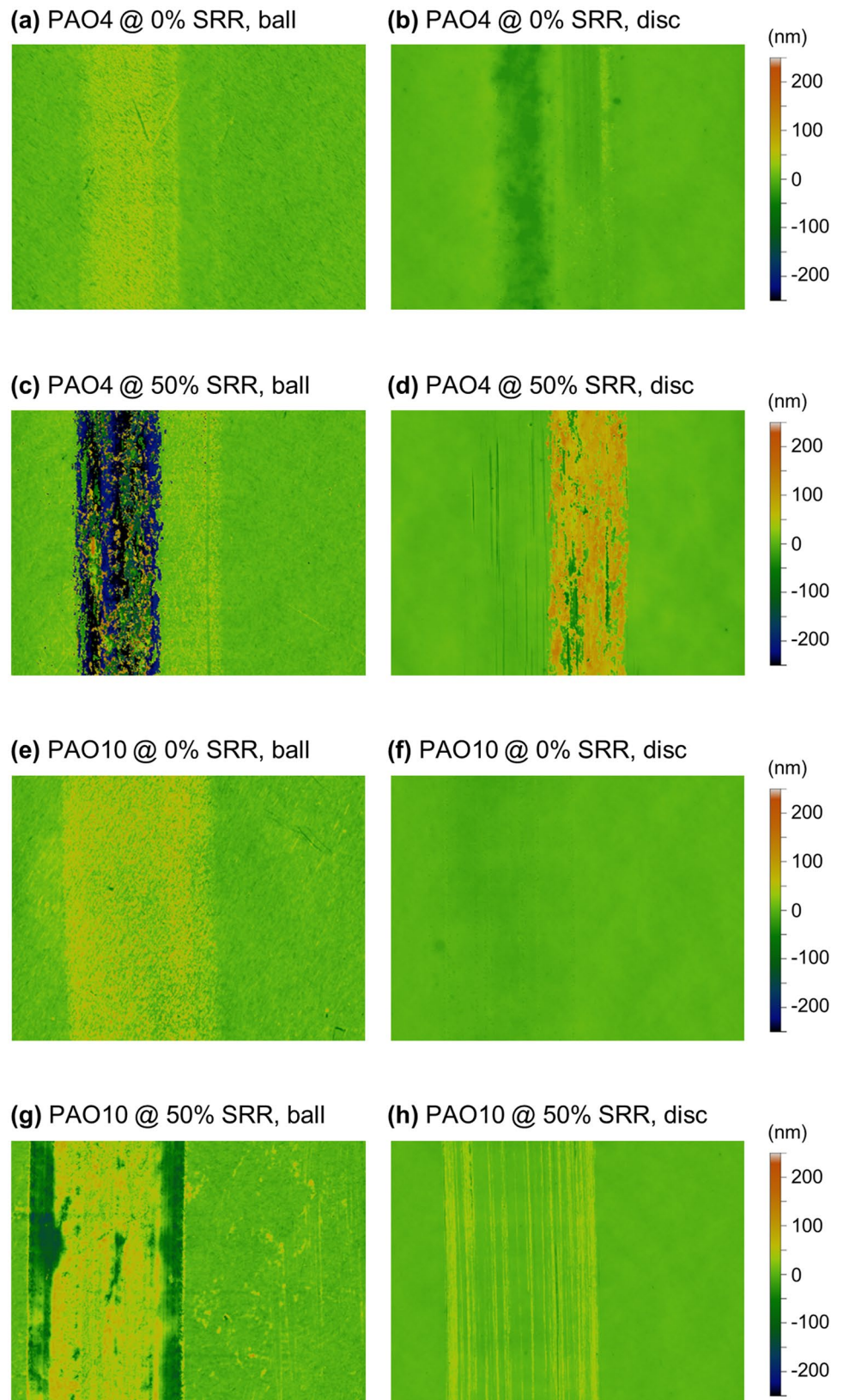
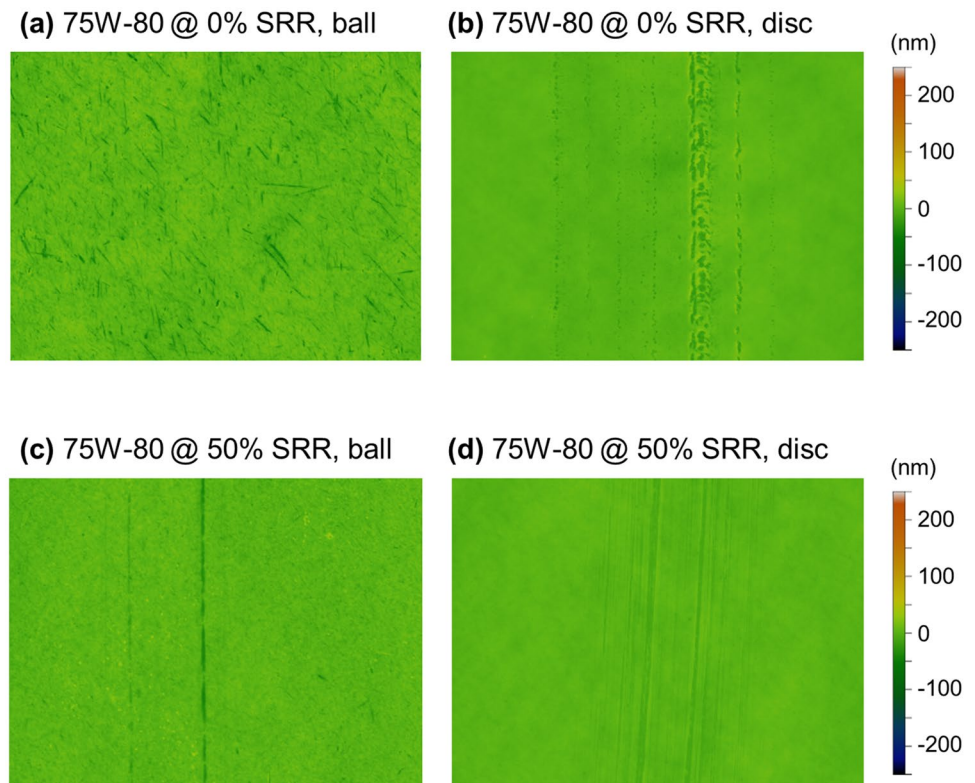


Fig. 7 WLI images ($700\ \mu\text{m} \times 530\ \mu\text{m}$, $\pm 250\ \text{nm}$ z-scale) for AuPd-coated MTM ball specimens (corrected for spherical curvature) and AuPd-coated disc specimens tested in 75W-80 at $100\ ^\circ\text{C}$, $1.12\ \text{GPa}$, and $150\ \text{mm/s}$ entrainment speed. Images **a**, **b** show the ball and disc steel surfaces, respectively, ran at 0% SRR. Images **c**, **d** similarly show the ball/disc pair ran at 50% SRR



3.3 ZrO_2/Co -Additive Antiwear Performance: Tribological Behavior

To better understand the origins of observed ZrO_2/co -additive interactions, it is useful to quantify the extent of the underlying surface wear discussed for Fig. 3. This is possible by calculating the WLI-measured step-edge heights and comparing these values to the tribofilm thicknesses measured in SLIM. Figure 8a plots the step-edge heights as a function of SRR, with the error bars representing the standard deviation between two replicate trials for each sample/

SRR. Figure 8b then shows the estimated wear depth, calculated by taking the difference between tribofilm thickness (Fig. 2g) and step-edge height (Fig. 8a).

Figure 8 supports the qualitative conclusions drawn from Fig. 3: that the presence of co-additives decreases the overall estimated wear of ZrO_2 -containing oils for the same SRR and λ values. For both PAO samples, the linear decrease in step-edge height with increasing SRR reflects a linear increase in estimated wear depth with increasing SRR due to nominally constant film thicknesses across SRR. Depending on the SRR, there is two to ten times less wear observed for

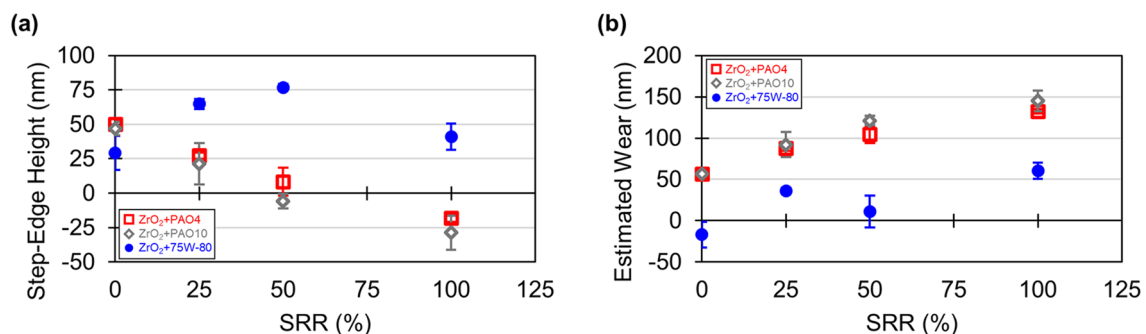


Fig. 8 The average tribofilm step-edge height for each sample/SRR shown in Fig. 3 is plotted in (a), where $\text{ZrO}_2+\text{PAO4}$ is red squares, $\text{ZrO}_2+\text{PAO10}$ is gray diamonds, and $\text{ZrO}_2+75\text{W-80}$ is blue circles. Using the difference from the tribofilm thicknesses measured in

SLIM and the step-edge heights measured in WLI, **b** plots the estimated wear depths as a function of SRR ($\text{ZrO}_2+\text{PAO4}$ is red squares, $\text{ZrO}_2+\text{PAO10}$ is gray diamonds, and $\text{ZrO}_2+75\text{W-80}$ is blue circles) (Color figure online)

ZrO₂+75W-80 vs ZrO₂+PAO10. Thus, importantly, despite varying extents of underlying surface wear, the ZrO₂ NPs play a beneficial role. This is especially evident in comparing the ZrO₂+PAO4 with the ZrO₂+75W-80 formulations. While the ZrO₂ alone still acts to prevent scuffing in PAO4, the additives work in a cooperative fashion, with no apparent antagonistic interactions, so that early scuffing and wear are mitigated in 75W-80.

Also importantly, while some wear is observed for ZrO₂+75W-80 whereas minimal surface changes occur in 75W-80 alone, this is a secondary point, as is the earlier observation that addition of NPs to 75W-80 can increase friction in MTM tests; the primary point is that macroscale tests have demonstrated improvements in, e.g., scuffing performance for when ZrO₂ is added to 75W-80 [33]. Thus, ZrO₂ NPs can act as an enabler for lower viscosity gear oils such as the 75W-80 oil studied here.

3.4 ZrO₂/Co-Additive Antiwear Performance: Chemical Analysis

Chemical analysis of the ZrO₂ tribofilms supports the contention that the substantial improvement in tribological behavior stems from the presence of both ZrO₂ and co-additives. Raman spectra (Fig. 9a) for tribofilms formed at a 50% SRR show distinct peaks for the ZrO₂+75W-80 sample relative to a tribofilm formed running in ZrO₂+PAO4. General assignments are that peaks < 900 cm⁻¹ arise from the ZrO₂ film and steel substrate [38–40] and peaks ~ 1000–17,000 cm⁻¹ arise from organic compounds, e.g., phosphate-containing species [41–43]. The peaks at 1060 cm⁻¹ and 1400 cm⁻¹ are only present in the ZrO₂+75W-80 tribofilm.

To further demonstrate the incorporation of co-additives into the tribofilm, the ZrO₂+PAO4 and ZrO₂+75W-80 derived tribofilms at 50% SRR were analyzed with secondary ion mass spectrometry (SIMS) depth profiling. The SIMS depth profiles of Fig. 9b,c are intrinsically relative

rather than absolute, but nonetheless, SIMS depth profiling does indicate apparently thicker tribofilms than measured in SLIM (Fig. 2g), based on the depth at which the Fe saturates and the Zr tapers. This difference is particularly pronounced for the ZrO₂+PAO4 film, with a 115 nm thick film measured in SLIM and approximately a 250 nm thick film measured in SIMS. However, film thicknesses in SIMS must be approached with care when roughness is present. It is possible that this apparent discrepancy occurs because the apparent depth in the SIMS is affected by the roughening of the steel that we have established occurs before the tribofilm nucleates and grows; this is especially a concern for the ZrO₂+PAO4 sample. This roughened buried interface will convolute signals from the film and the substrate in the SIMS measurements, with randomly located deeper valleys extending the tails of the Fe and Zr signals. In other words, while SLIM provides the average tribofilm thickness, the extent of the Fe and Zr signals is elongated by the presence of deeper valleys. The influence of a roughened interface on the apparent depth is qualitatively supported by comparison to the ZrO₂ tribofilm formed in 75W-80. The ZrO₂+75W-80 films typically have a less striated surface morphology, with less underlying wear, and there is correspondingly improved agreement between the film thickness measured by SLIM (90 nm) and the SIMS depth profiling (125 nm).

Like the SIMS measured depths, the SIMS concentrations are only estimates, not calibrated quantities. The relative amounts of each element can be directly compared between the two samples, but are not indicative of absolute values. Focusing on chemical content as a relative function of depth, phosphorus and sulfur are present throughout the tribofilm formed from ZrO₂+75W-80 (the dotted curves in Fig. 9c). Meanwhile, zirconium tapers off as the levels of iron grow, which indicates the transition from the tribofilm/wear track to the steel substrate (Fig. 9b). The trace amount of P and S observed for ZrO₂+PAO4 (solid lines in Fig. 9c) could originate from contamination or the 52,100 steel, but

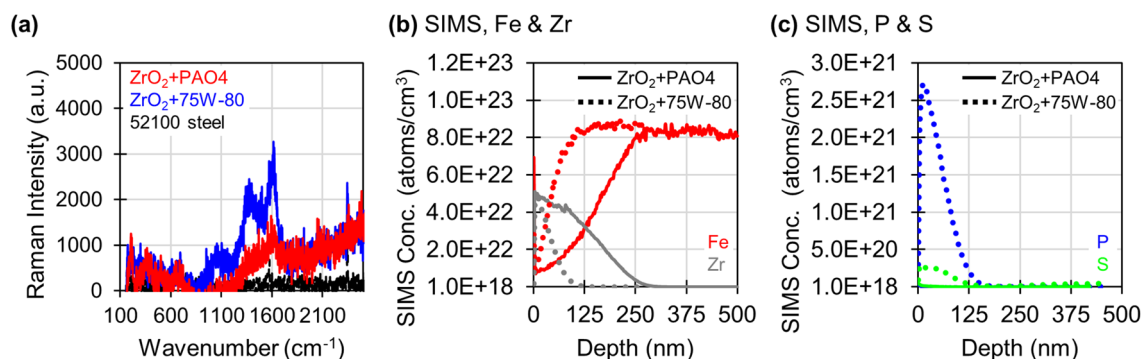


Fig. 9 **a** Raman spectra of tribofilms formed at a 50% SRR from ZrO₂+PAO4 (red), ZrO₂+75W-80 (blue), and a bare steel reference (black). **b** and **c** SIMS depth profiling data for ZrO₂+PAO4 (solid

lines) and ZrO₂+75W-80 (dotted lines) at a 50% SRR. **b** Shows Fe (red) and Zr (gray). **c** Shows P (blue) and S (green) (Color figure online)

is orders of magnitude lower than the amount of P and S present in ZrO₂+75W-80, underscoring the incorporation of P/S containing co-additives. Carbon content was also measured, and for both samples remained in a constant range of 4-to-7 × 10²¹ atoms/cm³ as a function of depth, a value 10 times lower than the maximum measured Zr concentration. This behavior for C content corroborates previous observations that the capping ligands are removed during tribofilm formation [16], and indicates that ligand removal is not affected by the co-additives in the gear oil.

Based on these results, the proposed mechanism for the tribological behavior when co-additives are present along with ZrO₂ is as follows. At the outset of the testing, co-additives adsorb to the surface and prevent initial scuffing and wear in the absence of the yet-to-be-formed ZrO₂ film, which requires some degree of contact before it forms [5, 6, 8, 9]. The additives are then incorporated into the ZrO₂ tribofilm as it is formed via tribosintering. The tribofilms formed in ZrO₂+75W-80 are thinner than those formed in PAO, which may affect film properties. While Raman and SIMS analysis confirm the presence of co-additives within the ZrO₂ tribofilm, these analytical methods do not shed insight into the internal film structure, nor the final crystal phase or exact chemical composition and bonding state. Determining the nature of the internal film requires substantial further study including utilizing microstructure analysis (e.g., via cross-sectional TEM) and investigating the possible occurrence of any tribochemical reactions (e.g., via XPS). This will be the focus of future work. Further work is also needed to determine potential long-term benefits from any altered crystal structure within the tribofilm. Our primary result here is to show that the addition of ZrO₂ NPs into a fully formulated 75W-80 gear oil, which is known to provide beneficial resistance to scuffing [33], exhibits cooperative behavior between the NPs and the EP additives. In particular, the ZrO₂-based tribofilms still grow as rapidly as they do in pure PAO, but the EP additives reduce wear of the steel surfaces that occur at the initial stages of contact before the tribofilm has formed.

4 Conclusions

One way to enable low viscosity gear oils for enhanced energy efficiency is to improve the quality of AW and EP additives; these additives should not interact antagonistically with existing lubricant co-additives, and furthermore should improve the tribological performance of a system. ZrO₂ NPs, attractive due to their stable, optically clear dispersions, demonstrate tribofilm formation under boundary contact conditions in both base oils and alongside co-additives. Prior work has shown that scuffing can be prevented by the use of these NPs [33]. Furthermore, tribofilms develop across

a range of slide-to-roll ratios, including rolling conditions (0% SRR). Though the tribofilm formation was consistently observed, based on a comparison of tribofilm thicknesses to tribofilm step-edge heights, initial surface wear appeared to occur before and/or during tribofilm growth. The severity of this underlying surface wear depended on the SRR and oil formulation. In samples comprising ZrO₂ in pure base oil (PAO4 and PAO10), while the eventual tribofilm thickness was independent of the SRR, the wear depth increased linearly with the SRR. The same experimental parameters for ZrO₂ in the fully formulated 75W-80 gear oil showed a substantial, twofold reduction in underlying surface wear, credited to cooperation between the EP additives and the ZrO₂ NPs. The EP additives provide initial protection against scuffing during ZrO₂ tribofilm formation, followed by interactions between ZrO₂ and gear oil co-additives. Chemical analysis indicates that P/S co-additives are present in the ZrO₂ tribofilm, suggesting that the combined effects of both ZrO₂ and co-additives are responsible for the enhanced tribological performance [33].

Acknowledgements We gratefully acknowledge support from the U.S. Army Combat Capabilities Development Command Ground Vehicle Systems Center (CCDC GVSC) under Small Business Technology Transfer (STTR) Phase II Award Number DE-SC-0009222. This work was also performed in part at the University of Pennsylvania's Singh Center for Nanotechnology, an NNCI member supported by NSF Grant ECCS-1542153. Elinski, M. B. acknowledges support from the University of Pennsylvania Provost Postdoctoral Fellowship program. We also thank Pixelligent Technologies, LLC for providing the oil formulations. The authors are appreciative of many useful discussions with N. G. Demas and B. J. Gould at Argonne National Laboratory, S. J. Thrush and A. S. Comfort at the U.S. Army CCDC GVSC, J. Lohuis and S. G. Williams (Pixelligent Technologies, LLC), Z. B. Milne (University of Pennsylvania), and H. S. Khare (formerly at the University of Pennsylvania, now at Gonzaga University).

Funding U.S. Army Combat Capabilities Development Command Ground Vehicle Systems Center (CCDC GVSC) Small Business Technology Transfer (STTR) Phase II Award Number DE-SC-0009222. University of Pennsylvania's Singh Center for Nanotechnology, an NNCI member supported by NSF Grant ECCS-1542153. Elinski, M. B. acknowledges support from the University of Pennsylvania Provost Postdoctoral Fellowship program.

Compliance with Ethical Standards

Conflict of interest Lei Zheng, Andrew Jackson, Robert J. Wiacek are affiliated with the commercial vendor for the ZrO₂ nanoparticles (Pixelligent Technologies, LLC). L. Z. and R. J. W. are employees of Pixelligent and have equity in the company. A. J. is a consultant to Pixelligent. No other coauthors declare competing financial interest.

References

1. Kakavas, I., Olver, A.V., Dini, D.: Hypoid gear vehicle axle efficiency. *Tribol. Int.* **101**, 314–323 (2016)

2. Holmberg, K., Andersson, P., Nylund, N.O., Makela, K., Erdemir, A., Global, A.: Global energy consumption due to friction in trucks and buses. *Tribol. Int.* **78**, 94–114 (2014)
3. International Energy Outlook, Tables A2 and A5. U.S. Energy Information Administration (2019)
4. Energy Flow Charts: Estimated World Energy Consumption in 2011. Lawrence Livermore National Laboratory (2011)
5. Stachowiak, G.W., Batchelor, A.W.: *Engineering Tribology*, 4th edn. Elsevier Inc, Amsterdam (2014)
6. Rizvi, S.: MNL59-EB A Comprehensive Review of Lubricant Chemistry, Technology, Selection, and Design. ASTM International, West Conshocken, PA (2009). <https://doi.org/10.1520/MNL59-EB>
7. Rudnick, L.R.: *Lubricant Additives: Chemistry and Applications*, 2nd edn. CRC Press Taylor & Francis Group, Boca Raton (2009)
8. Tuszyński, W., Michalczyński, R., Piekoszewski, W., Szczerek, M.: Modern automotive gear oils - classification, characteristics, market analysis, and some aspects of lubrication. In: Chiaberge, M. (ed.) *New Trends and Developments in Automotive Industry*. IntechOpen (2011). <https://doi.org/10.5772/13014>
9. Johnson, D.W., Hils, J.E.: Phosphate esters, thiophosphate esters and metal thiophosphates as lubricant additives. *Lubricants*. **1**, 132–148 (2013)
10. Shahnazar, S., Bagheri, S., Hamid, S.B.A.: Enhancing lubricant properties by nanoparticle additives. *Int. J. Hydrogen Energy*. **41**, 3153–3170 (2016)
11. Dai, W., Kheireddin, B., Gao, H., Liang, H.: Roles of nanoparticles in oil lubrication. *Tribol. Int.* **102**, 88–98 (2016)
12. Bakunin, V.N., Suslov, A.Y., Kuzmina, G.N., Parenago, O.P., Topchiev, A.V.: Synthesis and application of inorganic nanoparticles as lubricant components—a review. *J. Nanopart. Res.* **6**, 273–284 (2004)
13. Gulzar, M., Masjuki, H.H., Kalam, M.A., Varman, M., Zulkiffi, N.W.M., Mufti, R.A., Zahid, R.: Tribological performance of nanoparticles as lubricating oil additives. *J. Nanopart. Res.* **18**, 223 (2016)
14. Zhou, S., Garnweitner, G., Niederberger, M., Antonietti, M.: Dispersion behavior of zirconia nanocrystals and their surface functionalization with vinyl group-containing ligands. *Langmuir* **23**, 9178–9187 (2007)
15. Thrush, S.J., Comfort, A.S., Dusenbury, J.S., Xiong, Y., Qu, H., Han, X., Schall, J.D., Barber, G.C., Wang, X.: Stability, thermal conductivity, viscosity, and tribological characterization of zirconia nanofluids as a function of nanoparticle concentration. *Tribol. Trans.* **63**, 68–76 (2019)
16. Khare, H.S., Lahouji, I., Jackson, A., Feng, G., Chen, Z., Cooper, G.D., Carpick, R.W.: Nanoscale generation of robust solid films from liquid-dispersed nanoparticles via in situ atomic force microscopy: growth kinetics and nanomechanical properties. *ACS Appl. Mater. Interfaces* **10**, 40335–40347 (2018)
17. Ma, S., Zheng, S., Cao, D., Guo, H.: Anti-wear and friction performance of ZrO₂ nanoparticles as lubricant additive. *Particuology*. **8**, 468–472 (2010)
18. Battez, A.H., Gonzalez, R., Viesca, J.L., Fernandez, J.E., Fernandez, J.M.D., Machado, A., Chou, R., Riba, J.: CuO, ZrO₂ and ZnO nanoparticles as antiwear additive in oil lubricants. *Wear* **265**, 422–428 (2008)
19. Kato, H., Komai, K.: Tribofilm formation and mild wear by tribo-sintering of nanometer-sized oxide particles on rubbing steel surfaces. *Wear* **262**, 36–41 (2007)
20. Spikes, H.: The history and mechanisms of ZDDP. *Tribol. Lett.* **17**, 469–489 (2004)
21. Khare, H.S., Gosvami, N.N., Lahouji, I., Milne, Z.B., McClimon, J.B., Carpick, R.W.: Nanotribological printing: a nanoscale additive manufacturing method. *Nano Lett.* **18**, 6756–6763 (2018)
22. Acharya, B., Avva, K.S., Thapa, B., Pardue, T.N., Krim, J.: Synergistic effect of nanodiamond and phosphate ester antiwear additive blends. *Lubricants*. **6**, 56 (2018)
23. Khajeh, A., Krim, J., Martini, A.: Synergistic effect of nanodiamonds on the adsorption of tricresyl phosphate on iron oxide surfaces. *Appl. Phys. Lett.* **114**, 171602 (2019)
24. Rensselaar, J.V.: Extreme pressure/antiwear additives and friction modifiers. *Tribol. Lubr. Technol.* **74**, 24–28 (2018)
25. Morina, A., Neville, A., Priest, M., Green, J.H.: ZDDP and MoDTC interactions and their effect on tribological performance—tribofilm characteristics and its evolution. *Tribol. Lett.* **24**, 243 (2006)
26. de Barros-Bouchet, M.I., Martin, J.M., Le-Mogne, T., Vacher, B.: Boundary lubrication mechanisms of carbon coatings by MoDTC and ZDDP additives. *Tribol. Int.* **38**, 257–264 (2005)
27. Williams, Z.S.G., Wang, Y., Wiacek, R.J., Bai, X., Gou, L., Thomas, S.I., Xu, W., and Xu, J., Synthesis, capping and dispersion of nanocrystals. WO/2011/133228 (2011).
28. Williams, Z.S.G., Wang, Y., Wiacek, R.J., Bai, X., Gou, L., Thomas, S.I., Xu, W., and Xu, J., Synthesis, capping and dispersion of nanocrystals. WO/2012/058271 (2012).
29. Holder, C., Schaak, R.E.: Tutorial on powder X-ray diffraction for characterizing nanoscale materials. *ACS Nano* **13**, 7359–7365 (2019)
30. Jerman, M., Qiao, Z., Mergel, D.: Refractive index of thin films of SiO₂, ZrO₂, and HfO₂ as a function of the films' mass density. *Appl. Opt.* **44**, 3006–3012 (2005)
31. Dawczyk, J., Morgan, N., Russo, J., Spikes, H.: Film thickness and friction of ZDDP tribofilms. *Tribol. Lett.* **67**, 34 (2019)
32. Necas, D., Klapetek, P.: Gwyddion: an open-source software for SPM data analysis. *Cent. Eur. J. Phys.* **10**, 181–188 (2012)
33. Demas, N.G., Gould, B.J., Greco, A.C., Lorenzo-Martin, C., Erck, R.A., and Ajayi, O.O., Scuffing performance of low-viscosity gear oil containing ZrO₂ nanocrystals. *Proc. STLE/ASME Int. Jt. Tribol. Conf.* (2019)
34. Dai, W., Kheireddin, B., Gao, H., Kan, Y., Clearfield, A., Liang, H.: Formation of anti-wear tribofilms via alpha-ZrP nanoplatelet as lubricant additives. *Lubricants*. **4**, 1–12 (2016)
35. Zhang, J., Spikes, H.: On the mechanism of ZDDP antiwear film formation. *Tribol. Lett.* **63**, 24 (2016)
36. Vadiraj, A., Manivasagam, G., Kamani, K., Sreenivasan, V.S.: Effect of nano oil additive proportions on friction and wear performance of automotive materials. *Tribol. in Industry*. **34**, 3–10 (2012)
37. Hutchings, I., Shipway, P.: Wear by hard particles. In: *Tribology (Second Edition): Friction and Wear of Engineering Materials*, pp. 165–236. Butterworth-Heinemann (2017). <https://doi.org/10.1016/B978-0-08-100910-9.00006-4>
38. Wang, A., Haskin, L.A., Lane, A.L., Wdowiak, T.J., Squyres, S.W., Wilson, R.J., Hovland, L.E., Manatt, K.S., Raouf, N., Smith, C.D.: Development of the mars microbeam raman spectrometer (MMRS). *J. Geophys. Res.* **108**, 5005 (2003)
39. Barberis, P., Merle-Mejean, T., Quintard, P.: On Raman spectroscopy of zirconium oxide films. *J. Nucl. Mater.* **246**, 232–242 (1997)
40. Maczka, M., Lutz, E.T.G., Verbeek, H.J., Oskam, K., Meijerink, A., Hanuza, J., Stuiyinga, M.: Spectroscopic studies of dynamically compacted monoclinic ZrO₂. *J. Phys. Chem. Solid.* **60**, 1909–1914 (1999)

41. He, X., Xiao, H., Choi, H., Diaz, A., Mosby, B., Clearfield, A., Liang, H.: Alpha-zirconium phosphate nanoplatelets as lubricant additives. *Colloids Surf. A* **452**, 32–38 (2014)
42. Johnson, D.W., et al.: Application of Raman spectroscopy to lubricants, lubricated surfaces, and lubrication phenomena. *Spectroscopy*. **26**, 1–4 (2011)
43. Singh, H., Ramirez, G., Eryilmaz, O., Greco, A., Doll, G., Erdemir, A.: Fatigue resistant carbon coatings for rolling/sliding contacts. *Tribol. Int.* **98**, 172–178 (2016)

Publisher's Note Springer Nature remains neutral with regard to jurisdictional claims in published maps and institutional affiliations.